applied sciences

MDPI

Article

Design of Cold-Formed Steel Screw Connections with Gypsum Sheathing at Ambient and Elevated Temperatures

Wei Chen [1,*], Jihong Ye [1] and Tao Chen [2]

[1] Key Laboratory of Concrete and Prestressed Concrete Structures of the Ministry of Education, Southeast University, Nanjing 210096, China; yejihongseu@163.com

[2] Nanjing University of Science and Technology, Nanjing 210000, China; chentao@njust.edu.cn

* Correspondence: weichen@seu.edu.cn; Tel.: +86-25-8379-4253

Academic Editor: Zhong Tao

Received: 16 June 2016; Accepted: 30 August 2016; Published: 6 September 2016

Abstract: Load-bearing cold-formed steel (CFS) walls sheathed with double layers of gypsum plasterboard on both sides have demonstrated good fire resistance and attracted increasing interest for use in mid-rise CFS structures. As the main connection method, screw connections between CFS and gypsum sheathing play an important role in both the structural design and fire resistance of this wall system. However, studies on the mechanical behavior of screw connections with double-layer gypsum sheathing are still limited. In this study, 200 monotonic tests of screw connections with single- or double-layer gypsum sheathing at both ambient and elevated temperatures were conducted. The failure of screw connections with double-layer gypsum sheathing in shear was different from that of single-layer gypsum sheathing connections at ambient temperature, and it could be described as the breaking of the loaded sheathing edge combined with significant screw tilting and the loaded sheathing edge flexing fracture. However, the screw tilting and flexing fracture of the loaded sheathing edge gradually disappear at elevated temperatures. In addition, the influence of the loaded edge distance, double-layer sheathing and elevated temperatures is discussed in detail with clear conclusions. A unified design formula for the shear strength of screw connections with gypsum sheathing is proposed for ambient and elevated temperatures with adequate accuracy. A simplified load–displacement model with the post-peak branch is developed to evaluate the load–displacement response of screw connections with gypsum sheathing at ambient and elevated temperatures.

Keywords: cold-formed steel; screw connections; experimental investigation; elevated temperature; double-layer gypsum sheathing; design formulas

1. Introduction

In recent years, load-bearing cold-formed steel (CFS) walls sheathed with gypsum plasterboard on either side have been increasingly used in low- and mid-rise buildings. Screw fasteners that connect the CFS frame and gypsum sheathing have become the main connection method for this wall system. Due to the lateral constraints provided by the screw connections, the bearing capacity of a CFS frame can be significantly enhanced. To prevent failure of the sheathing-fastener-stud sheathing, the maximum nominal load for the screw connection was given for the all-steel design method of CFS wall studs in the design manual of American Iron and Steel Institute (AISI) [1]. Moreover, screw connections make the walls behave similarly to diaphragms resisting in-plane lateral loads (wind and seismic loads) [2]. Hence, the mechanical behavior of the screw connections plays an important role in the design of CFS walls.

Several experimental investigations [3–9] have already been conducted on the shear response of screw connections with gypsum sheathing or other board materials at ambient temperature.

Gypsum sheathing does not have a preferential material response in a specific direction [7], and the failure of screw connections with single-layer gypsum sheathing was mainly identified as breaking or bearing of the loaded sheathing edge [6–8]. Furthermore, the effect of the loading rate, steel thickness, loaded edge distance and loading protocol were also discussed with explicit conclusions [5–9]. Some mathematical models, such as the Foschi model [10], Pivot model [9,11] and Pinching 4 model [7], were used to describe the monotonic or cyclic load–displacement characteristic of connections at ambient temperature.

However, previous research [3–9] mainly focused on screw connections with only a single layer of sheathing material at ambient temperature. In mid-rise buildings, double layers of gypsum sheathing are necessary on both sides of load-bearing CFS walls to satisfy the fire resistance rating of at least 60 min [12–14]. The lateral resistance performance of CFS walls with double-layer gypsum sheathing on both sides has been shown to be different from that of walls with single-layer sheathing [15,16]. As described in the recently issued AISI standard [17], insufficient research exists to provide a definitive solution for the design of CFS walls with multiple layers of sheathing on an individual face of a wall. In addition, no literature was found regarding the shear response of screw fasteners with double-layer gypsum sheathing at ambient temperature. A few experiments were conducted on the mechanical behavior of CFS sheeting-fastener-sheeting connections at elevated temperatures [18–20]. However, investigation on the screw connections with board sheathing materials at elevated temperatures is still limited, so the mechanical contribution of gypsum sheathing in the previous theoretical and numerical investigation of CFS walls under fire conditions remains unknown [21,22].

According to the previous full-scale experiments [13], the loaded CFS wall assembly lined with double layers of gypsum plasterboard on both sides was subjected to the ISO834 fire exposure of 71 min, and the flexural deflection of steel studs increased rapidly towards the fire side at the final two minutes of fire exposure. Post-fire inspection showed that the fire-side gypsum plasterboard had good deformation compatibility with the CFS frame, and only few cracks were observed in the field of fire-side gypsum plasterboard. In addition, due to the shrinkage of gypsum and degenerated mechanical behavior of screw connections, the breaking of the loaded sheathing edge was identified along the periphery of the fire-side gypsum plasterboard, leading to the opening of vertical board joints. In this paper, it was assumed that the shear experiments of screw connections did not consider the effects of the cracking of gypsum plasterboard caused by the flexural deflection of the wall assembly at elevated temperatures. A detailed investigation of 200 monotonic tests was conducted for the screw connections with gypsum sheathing at ambient and elevated temperatures. The specimens were carefully designed to avoid the out-of-plane curling of the CFS coupon. The effects of the loaded edge distance and double layers of sheathing were discussed. The design formulas of some key parameters of screw connections as well as a simplified load–displacement model were developed at ambient and elevated temperatures to provide a reasonable basis for the design and the numerical simulation of CFS walls.

2. Test Program

2.1. Test Device

The shear experiments of CFS screw connections at ambient and elevated temperatures were conducted at Nanjing University of Science and Technology, China. The loading device was an electronic universal material testing machine (Changchun Research Institute for Mechanical Science Co. Ltd, Changchun, China) (Figure 1) with a loading capacity of 50 kN and strong stability at small levels of loading. The heating device (Changchun Research Institute for Mechanical Science Co. Ltd, Changchun, China) was a cylindrical electric furnace (Figure 1) with a cavity diameter of 85 mm and a cavity height of 280 mm. In addition, three type-K thermocouples were arranged around the loaded screw (Figures 2 and 3) of the specimen to ensure that the screw connection maintained the pre-set temperature.

Figure 1. Test system for the experiments.

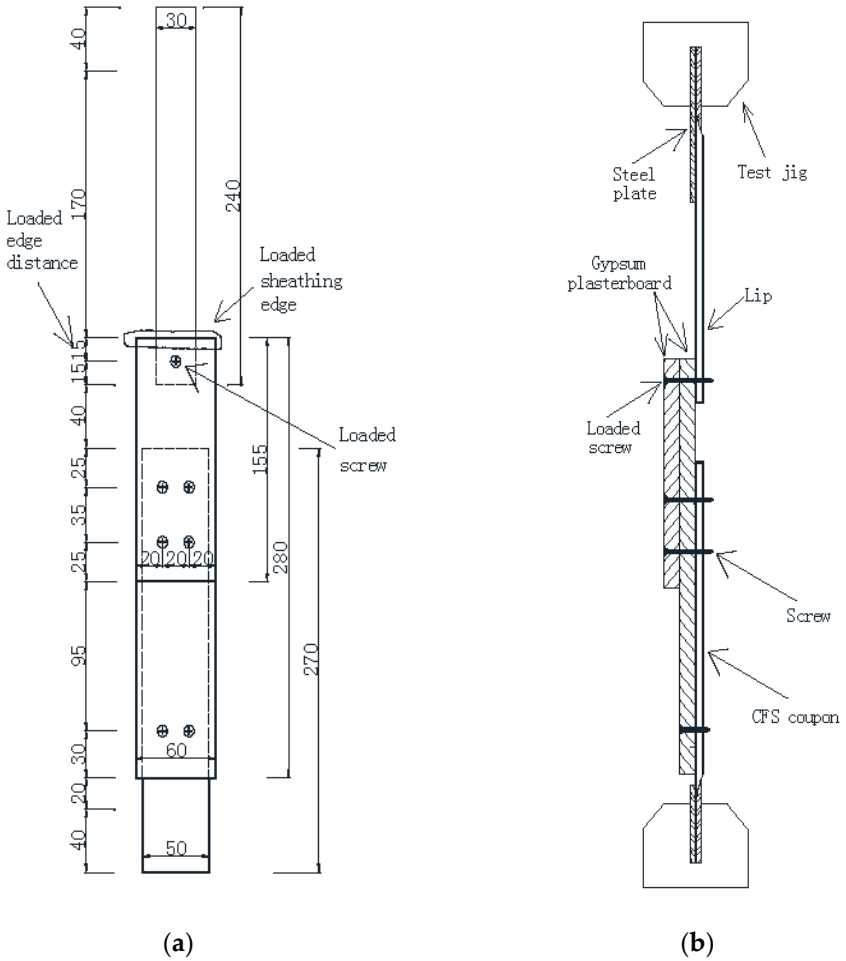

Figure 2. Connection details with double-layer sheathing and a loaded edge distance of 15 mm: (**a**) front view; and (**b**) side view.

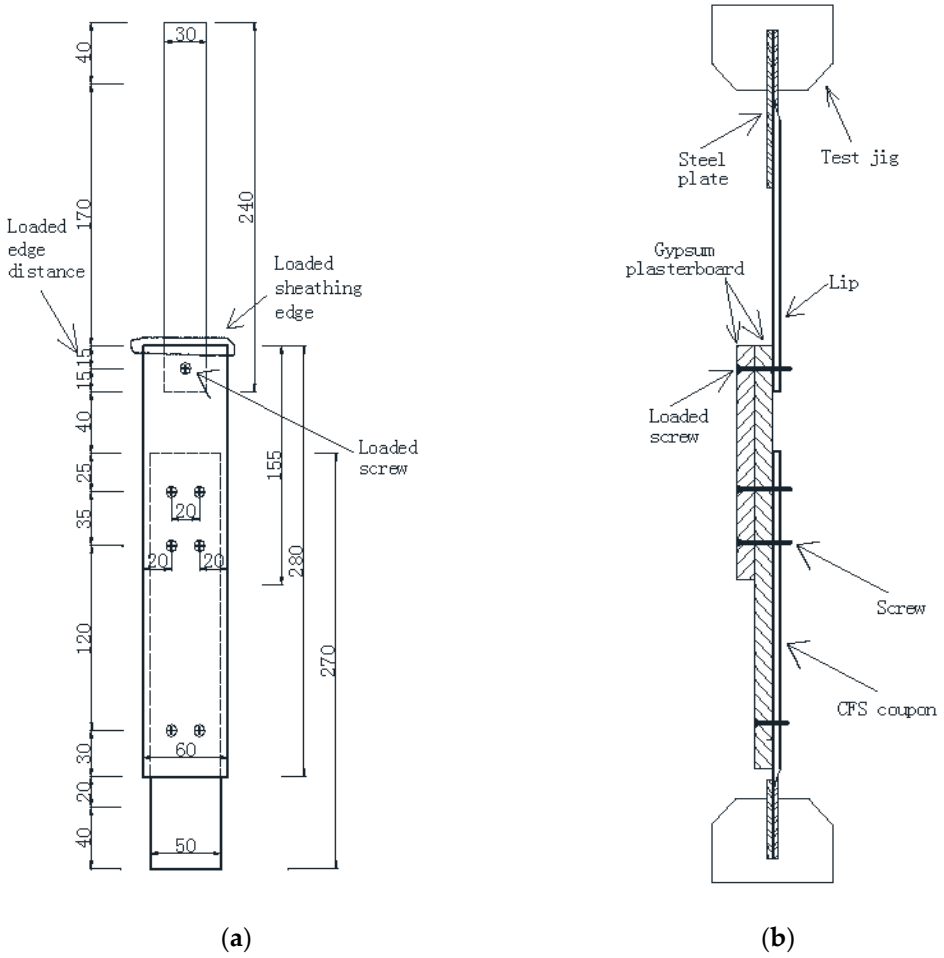

Figure 3. Connection details with single-layer sheathing and a loaded edge distance of 15 mm: (**a**) front view; and (**b**) side view.

2.2. Specimen Design and Assembly

Limited to the cavity dimensions of the furnace, the single-lap test of the CFS coupon-fastener-sheathing connections (Figures 2 and 3) was adopted in this paper. Compared to the test scheme of multi-screw stud-fastener-sheathing connections [6,7], the loaded sheathing edge of the coupon-fastener-sheathing connection had only one screw. Hence, high accuracy for the specimen assembly was easy to achieve, especially for the loaded edge distance, which might have an important influence on the shear behavior of screw connections with sheathing. According to the AISI design manual [17], the minimum distance of the loaded sheathing edge is 9.5 mm in the United States and 12.5 mm in Canada. Therefore, three loaded edge distances (10, 15 and 20 mm) were considered in the experiments. In addition, single and double layers of 12.5 mm thick fire-resistant gypsum plasterboard were attached to 1.0 mm thick G550 cold-formed steel by self-drilling bugle head screws. The screw diameter was 4.2 mm, which is the minimum size for screw connections of CFS structures in the Chinese design guide [23]. As shown in Figures 2 and 3, the lip was designed for the CFS coupon to avoid the out-of-plane curling of CFS sheets that was found in the previous shear experiments of CFS sheet-fastener-sheet connections [19], and this might affect the failure mode of the connections. In addition, two pieces of steel plates (Figures 2b and 3b) were used to grip the CFS coupon to restrict the out-of-plane deflection of CFS coupons at the testing rig.

Before assembly of the screw connection, the gypsum plasterboard needs to be cut into pieces and manually polished to ensure the smoothness of the loaded sheathing edge. Next, small holes were drilled by a 2 mm diameter drill bit for the gypsum plasterboard pieces and the CFS coupon at the

location of the loaded screw (Figures 2 and 3). Then, the gypsum plasterboard pieces and CFS coupon were fixed together using a screw to form the screw connection. Finally, the loaded edge distance of the assembled specimen was checked and adjusted by art knife, if necessary. Figure 4a shows a specimen with double layers of gypsum sheathing, and Figure 4b shows the verification of the loaded edge distance (20 mm) for that specimen.

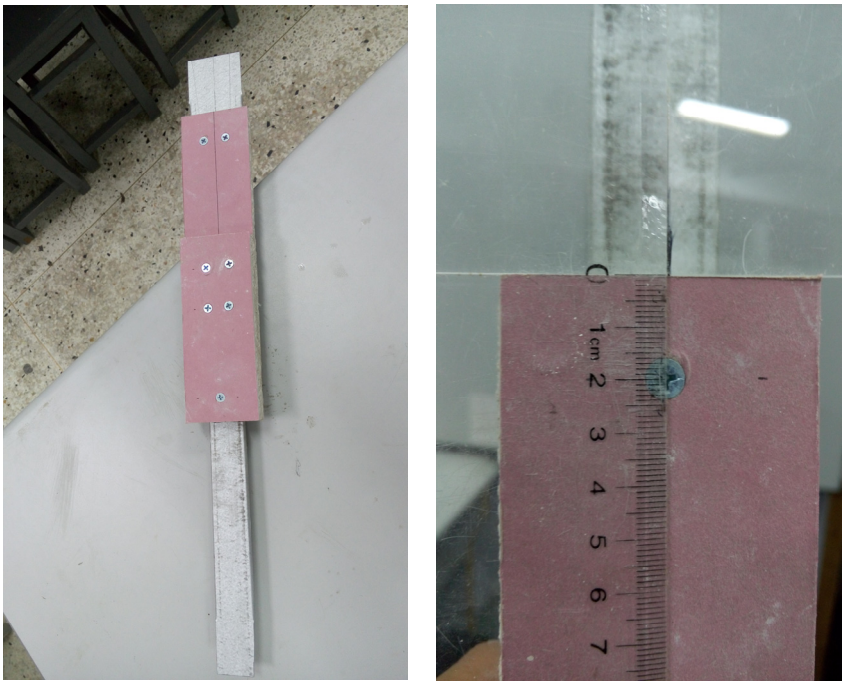

(**a**) (**b**)

Figure 4. A typical screw connection specimen: (**a**) side view; and (**b**) verification of the loaded edge distance (20 mm).

2.3. Test Procedure

The specimen was mounted into the loading machine by gripping the upper end of the specimen and relaxing the bottom end. Then, the furnace was heated to the pre-set temperature and held for 120 min at this constant temperature. Subsequently, the bottom end of the specimen was manually gripped, and a monotonic tension load was gradually applied to the specimen at a constant displacement rate of 0.025 mm/s until failure while maintaining the pre-set temperature.

A total of ten temperature levels were considered in the present experiments, including the ambient temperature (approximately 20 °C) and elevated temperatures from 100 °C to 500 °C at intervals of 50 °C. Based on the previous investigation, the shear experimental results of the screw connection with gypsum sheathing may be more scattered than the tension results of the CFS coupon [7]. In this paper, the shear strength of the connection was taken as the control parameter. A strict rule similar to ASTM (American Society for Testing and Materials) E2126-11 [24] was made to establish the number of nominally identical specimens for each series, and it is described as follows: (a) each series was started and repeated three times; (b) if the relative error between the strength of the generic specimen and the average strength of the series was less than 10%, the number of specimens for this series was three; (c) otherwise, a fourth test was performed, and if the relative error was less than 15%, the number of specimens for this series was four; and (d) otherwise, the number of specimens for this series was five. Therefore, three to five experiments were conducted for each series, and a total of 200 tests were performed in this study.

3. Test Results

3.1. General

For illustration, all of the specimens were labeled according to the following rule: the first group of characters represent the sheathing material (GPB: gypsum plasterboard); the second group of characters represent the loaded edge distance (10, 15 or 20 mm); the third group describes the number of layers for sheathing (S for single-layer or D for double-layer); and the last group indicates the temperature for the experiment (20 °C (ambient temperature) or 100 °C–500 °C). For instance, GPB20D-20 refers to a specimen with double layers of gypsum plasterboard and a loaded edge distance of 20 mm at ambient temperature. Figure 5 gives the typical load–displacement curve for the specimen GPB20D-20. Tables 1 and 2 summarize the average results and coefficient of variation (COV) for each series. F_{mT} represents the shear strength of the specimen at T °C; Δ_{mT} is the recorded displacement corresponding to F_{mT} at T °C; Δ_{uT} is the recorded displacement corresponding to $0.8F_{mT}$ on the post-peak branch of response at T °C; Δ_{eT} is the recorded displacement corresponding to $0.4F_{mT}$ at T °C; and K_{eT} is the initial shear stiffness of the screw connection at T °C and $K_{eT} = 0.4F_{mT}/\Delta_{eT}$. E_T represents the absorbed energy of the connection at T °C, which is the area under the load–displacement curve up to Δ_{uT}. In addition, the characters for the failure mode in Tables 1 and 2 were grouped as follows: *B* represents the breaking of the loaded sheathing edge (Figure 6a); *T* represents the screw tilting (Figure 7c); and *F* represents the flexing fracture of the sheathing (Figure 7c). For instance, B/B + T indicates the breaking of the loaded sheathing edge alone or combined with screw tilting. In Tables 1 and 2, the scatter of the test results is significant, except for F_{mT}. Both F_{mT} and K_{eT} of the screw connection decreased with increasing temperatures. However, K_{eT} of some series at 100 °C (for instance, GPB20S-100 and GPB15D-100) became much higher than that of the series at ambient temperature, and Δ_{mT} of the series at 100 °C became much lower than those of the series at ambient temperature and 150 °C. No reasonable explanation is currently offered for such a phenomenon. Moreover, Tables 1 and 2 show that the shear strength of the double-layer sheathing connection was higher than but not twice that of the shear strength of the single-layer sheathing connection. Therefore, the linear superposition method is not applicable, which should be taken into consideration in the design of CFS walls with double-layer sheathing. The effect of double-layer sheathing is discussed separately in this paper.

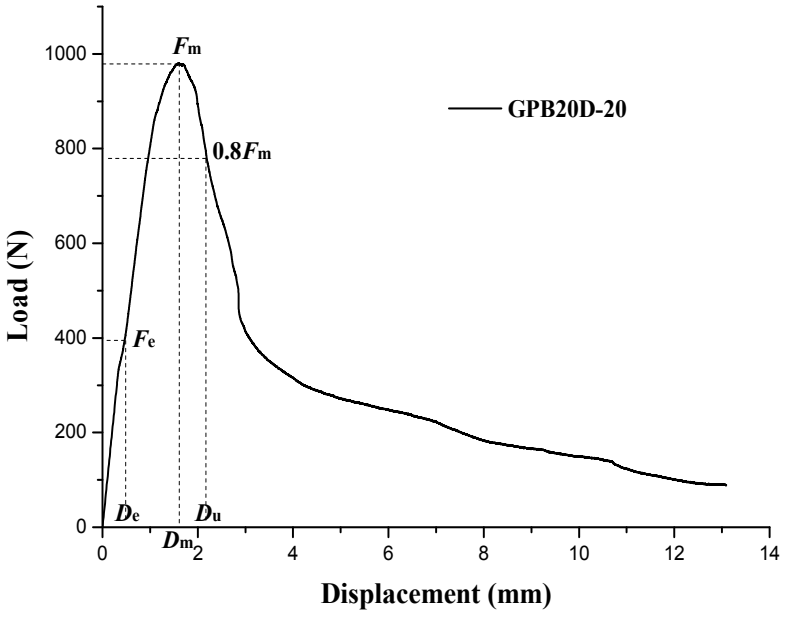

Figure 5. Typical load–displacement curve of (gypsum plasterboard) GPB20D-20.

Table 1. Experimental results of CFS screw connection with single-layer gypsum sheathing.

Specimen	k_{eT} (*N*/mm)		F_{mT} (*N*)		Δ_{eT} (mm)		Δ_{mT} (mm)		Δ_{uT} (mm)		E_T (N·mm)		Failure Mode
	Mean	COV	Mean	COV	Mean	COV	Mean	COV	Mean	COV	Mean	COV	
GPB10S-20	1215	39.0%	471	4.9%	0.175	46.0%	0.720	20.2%	1.274	3.4%	439	10.3%	B
GPB10S-100	1189	36.0%	385	3.8%	0.143	40.8%	0.457	37.4%	0.877	31.5%	251	28.5%	
GPB10S-150	495	6.7%	220	8.0%	0.179	13.7%	0.810	25.1%	1.305	16.0%	218	20.7%	
GPB10S-200	535	2.2%	170	5.4%	0.127	7.6%	0.452	36.3%	1.052	24.8%	139	32.7%	
GPB10S-250	440	19.6%	144	7.3%	0.133	13.8%	0.607	7.8%	1.282	8.2%	150	12.9%	
GPB10S-300	317	15.3%	122	1.7%	0.156	18.3%	0.603	7.2%	1.095	6.4%	102	9.3%	
GPB10S-350	253	10.1%	97	8.2%	0.150	18.9%	0.500	4.5%	0.813	5.9%	56	12.7%	
GPB10S-400	240	20.6%	107	10.4%	0.181	11.4%	0.657	19.4%	0.918	22.6%	71	35.7%	
GPB10S-450	185	6.5%	82	6.1%	0.173	10.6%	0.581	20.0%	0.728	18.3%	39	24.6%	
GPB10S-500	181	7.3%	74	8.8%	0.158	4.5%	0.492	16.7%	0.765	25.7%	38	25.0%	
GPB15S-20	857	17.3%	565	3.4%	0.268	13.4%	0.958	18.1%	1.406	7.7%	572	4.8%	B
GPB15S-100	962	19.2%	473	4.2%	0.202	23.2%	0.614	16.1%	0.816	15.2%	251	12.3%	
GPB15S-150	530	3.7%	326	7.0%	0.253	8.0%	0.725	11.8%	1.018	13.0%	226	16.2%	
GPB15S-200	592	23.2%	202	3.8%	0.143	29.2%	0.562	41.7%	1.006	39.2%	167	40.3%	
GPB15S-250	408	7.8%	161	8.1%	0.159	16.1%	0.574	30.8%	0.954	35.9%	114	45.4%	
GPB15S-300	386	11.8%	161	7.8%	0.170	20.1%	0.593	21.8%	1.032	16.1%	124	20.8%	
GPB15S-350	347	12.5%	140	7.6%	0.164	18.6%	0.540	10.8%	0.954	8.5%	101	14.8%	
GPB15S-400	301	8.7%	109	8.3%	0.145	2.9%	0.417	5.1%	0.532	0.3%	37	10.4%	
GPB15S-450	329	10.1%	132	6.8%	0.163	11.3%	0.502	11.1%	0.640	15.9%	55	19.9%	
GPB15S-500	314	20.4%	103	9.2%	0.136	34.3%	0.403	24.9%	0.496	22.0%	34	26.0%	
GPB20S-20	1004	23.4%	711	4.5%	0.292	17.6%	1.243	17.8%	1.672	14.5%	871	11.1%	B/B + T
GPB20S-100	1806	28.5%	637	1.6%	0.150	32.8%	0.511	18.0%	0.705	18.7%	307	20.2%	B
GPB20S-150	606	0.3%	379	6.9%	0.250	7.1%	0.896	6.8%	1.232	19.3%	318	23.4%	
GPB20S-200	671	18.6%	270	5.1%	0.165	20.9%	0.593	29.1%	0.792	29.0%	145	38.9%	
GPB20S-250	595	18.6%	201	2.8%	0.139	21.6%	0.617	12.8%	1.003	6.3%	156	4.8%	
GPB20S-300	536	15.3%	219	2.3%	0.178	18.7%	0.660	4.6%	1.048	7.1%	170	7.9%	
GPB20S-350	500	13.3%	182	8.6%	0.148	20.4%	0.558	50.3%	0.832	56.2%	109	71.7%	
GPB20S-400	468	18.1%	217	9.9%	0.189	21.8%	0.640	19.6%	0.921	20.3%	141	33.1%	
GPB20S-450	358	3.5%	177	3.4%	0.198	0.4%	0.555	4.3%	0.645	11.1%	70	16.1%	
GPB20S-500	295	11.2%	146	3.8%	0.207	18.2%	0.613	2.7%	0.719	2.4%	62	4.3%	

COV, coefficient of variation; CFS, cold-formed steel; GPB, gypsum plasterboard.

Table 2. Experimental results of CFS screw connection with double-layer gypsum sheathing.

Specimen	k_{eT} (N/mm)		F_{mT} (N)		Δ_{eT} (mm)		Δ_{mT} (mm)		Δ_{uT} (mm)		E_T (N·mm)		Failure Mode
	Mean	COV	Mean	COV	Mean	COV	Mean	Mean	COV	mean	COV	Mean	
GPB10D-20	1092	3.5%	663	1.9%	0.243	2.9%	0.974	8.5%	1.480	6.9%	740	6.6%	B + T + F
GPB10D-100	1251	17.7%	560	2.5%	0.182	15.9%	0.655	5.6%	0.962	3.2%	383	4.2%	
GPB10D-150	638	19.7%	321	6.4%	0.207	22.2%	1.122	13‘.3%	1.658	8.6%	408	11.9%	
GPB10D-200	714	15.3%	262	11.1%	0.149	17.5%	0.755	27.7%	1.674	16.2%	357	15.5%	
GPB10D-250	774	9.4%	226	3.3%	0.118	12.8%	0.999	31.2%	2.002	26.8%	377	30.8%	
GPB10D-300	648	22.0%	197	5.1%	0.126	22.3%	1.016	13.4%	2.046	4.3%	339	4.4%	B
GPB10D-350	527	12.6%	209	4.3%	0.161	15.1%	1.151	29.9%	2.028	20.5%	351	22.0%	
GPB10D-400	546	15.8%	145	10.0%	0.107	10.9%	0.798	39.3%	1.570	13.2%	193	24.1%	
GPB10D-450	329	18.0%	119	6.9%	0.149	23.0%	0.584	42.4%	1.213	3.2%	112	1.4%	
GPB10D-500	250	12.8%	88	5.6%	0.144	5.9%	0.728	32.1%	1.215	35.0%	87	48.6%	
GPB15D-20	1041	24.1%	753	3.5%	0.298	18.3%	1.327	8.7%	1.908	4.0%	1079	3.6%	B + T + F
GPB15D-100	1348	10.4%	681	1.7%	0.204	11.8%	0.770	8.3%	1.003	13.6%	479	15.5%	B + T + F
GPB15D-150	688	16.8%	443	5.2%	0.261	11.9%	0.849	15.3%	1.636	30.9%	515	28.2%	
GPB15D-200	671	10.6%	304	9.8%	0.188	16.9%	0.492	14.6%	1.368	9.0%	306	5.5%	
GPB15D-250	670	12.5%	229	7.5%	0.137	5.5%	0.999	14.3%	2.348	14.0%	469	20.2%	
GPB15D-300	706	19.3%	191	3.5%	0.112	24.8%	1.212	41.1%	2.669	10.4%	442	11.1%	B
GPB15D-350	613	34.7%	207	8.6%	0.150	38.4%	0.839	29.7%	1.959	19.0%	344	24.3%	
GPB15D-400	412	14.0%	144	7.4%	0.142	16.9%	0.745	81.6%	1.971	42.9%	217	42.9%	
GPB15D-450	323	12.6%	117	9.1%	0.146	14.4%	0.791	36.4%	1.388	25.9%	130	30.7%	
GPB15D-500	318	12.5%	112	3.1%	0.142	14.7%	0.796	28.6%	2.204	60.1%	209	68.7%	
GPB20D-20	1041	20.2%	998	3.3%	0.394	20.2%	1.653	10.8%	2.382	12.0%	1791	17.3%	B + T + F
GPB20D-100	1458	5.9%	928	5.5%	0.255	10.3%	0.971	21.5%	1.304	4.6%	857	9.4%	B + T + F
GPB20D-150	870	13.9%	694	5.6%	0.326	20.5%	1.573	17.5%	1.938	10.0%	949	15.9%	B + T + F
GPB20D-200	864	7.7%	464	4.8%	0.216	12.1%	0.695	14.9%	1.003	9.3%	318	10.0%	
GPB20D-250	987	13.0%	316	3.2%	0.130	16.8%	0.508	23.8%	2.444	15.1%	628	10.8%	
GPB20D-300	757	7.1%	304	9.7%	0.162	16.8%	0.545	35.2%	2.693	16.0%	686	20.3%	
GPB20D-350	795	22.4%	271	13.0%	0.139	13.0%	0.628	5.5%	1.420	17.4%	321	18.2%	B
GPB20D-400	650	10.2%	194	9.4%	0.120	12.3%	0.570	17.3%	1.873	11.3%	310	11.2%	
GPB20D-450	459	6.6%	187	8.2%	0.164	14.4%	0.440	17.4%	0.846	27.7%	110	31.4%	
GPB20D-500	413	9.2%	158	10.4%	0.154	17.6%	0.405	12.3%	0.955	26.3%	109	23.7%	

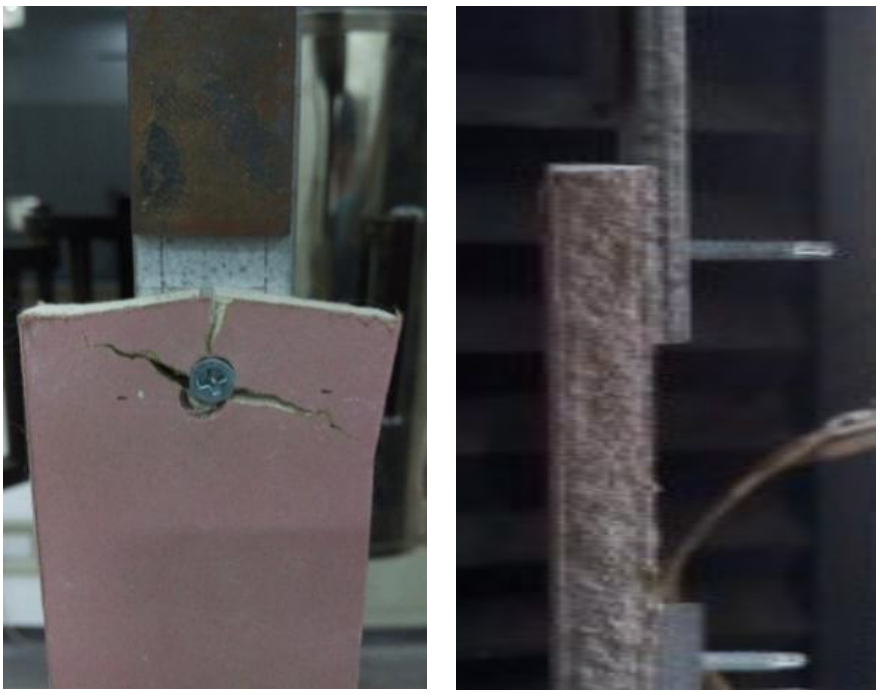

(**a**) (**b**)

Figure 6. Breaking of the loaded sheathing edge for GPB15S-20: (**a**) front view; and (**b**) side view.

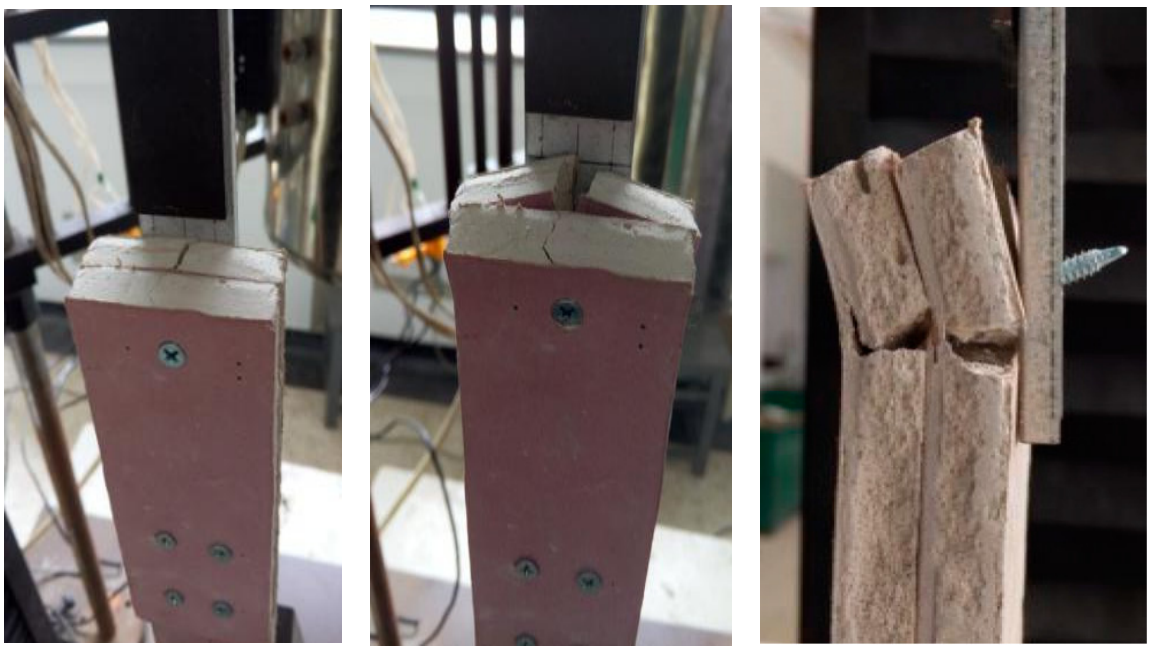

(**a**) (**b**) (**c**)

Figure 7. The failure process of GPB20D-20: (**a**) cracking of the base layer gypsum plasterboard on the loaded edge; (**b**) failure of the base layer gypsum plasterboard; and (**c**) B + T + F failure.

3.2. Visual Observation

For the single-layer gypsum sheathing connections at ambient temperature, cracks first appeared along the thickness of the loaded sheathing edge. With increasing deflection, the cracks grew on the gypsum surface around the loaded screw (Figure 6) until losing the shearing capacity of the screw connection.

The failure process for the double-layer sheathing connection was different from that of the single-layer sheathing connection at ambient temperature. Cracking first appeared on the loaded sheathing edge of the base layer plasterboard (Figure 7a) because the base layer gypsum plasterboard was subjected to the bearing of the screw hole–wall oriented towards the loaded sheathing edge. The bearing of the screw hole–wall for the face layer gypsum plasterboard was oriented towards the field of sheathing. Following the crack propagation, failure of the base layer plasterboard (Figure 7b) occurred while the face layer plasterboard still had not lost its bearing capacity. Therefore, the deflection capacity of the double-layer sheathing connection is much higher than that of the single-layer sheathing connection, as shown in Figure 8.

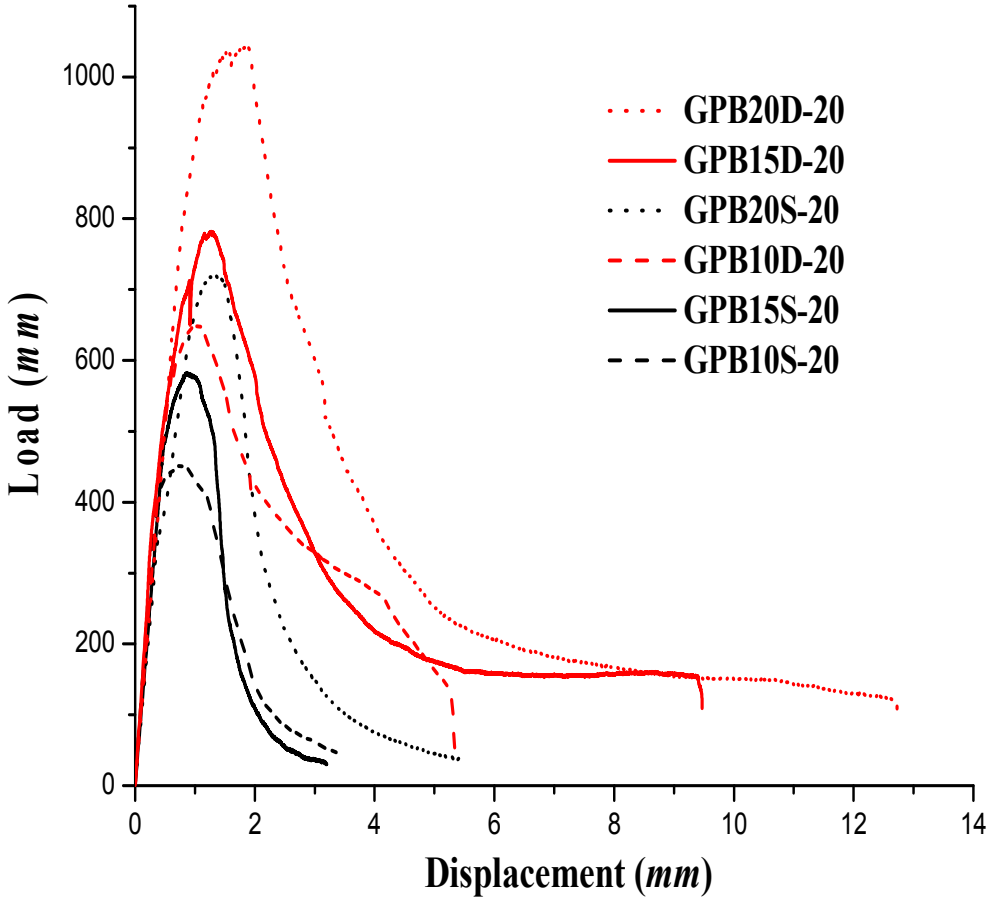

Figure 8. Load–displacement curves of the connection series at ambient temperature.

For the connection series at elevated temperatures, the off-test inspection indicated that the color of the paper facing on the gypsum plasterboard remained stable below 150 °C (Figures 9a and 10a) and gradually changed to light gray (200 °C, Figures 9b and 10b), black (250 °C, Figures 9c and 10c), off-white (400 °C, Figures 9f and 10f) and white (450 °C, Figures 9g and 10g) with increasing temperature. In addition, the paper facing on the gypsum plasterboard maintained integrity below 250 °C and significantly cracked at 300 °C (Figures 9d and 10d). Beyond 350 °C (Figures 9e and 10e), the paper facing on the gypsum plasterboard began to fall off. Therefore, the sharp degeneration of the shear strength of the connection series at 150 °C (Tables 1 and 2) was likely due to the dehydration of the gypsum, and the effect of the paper facing on the shear behavior of the connection became insignificant beyond 300 °C.

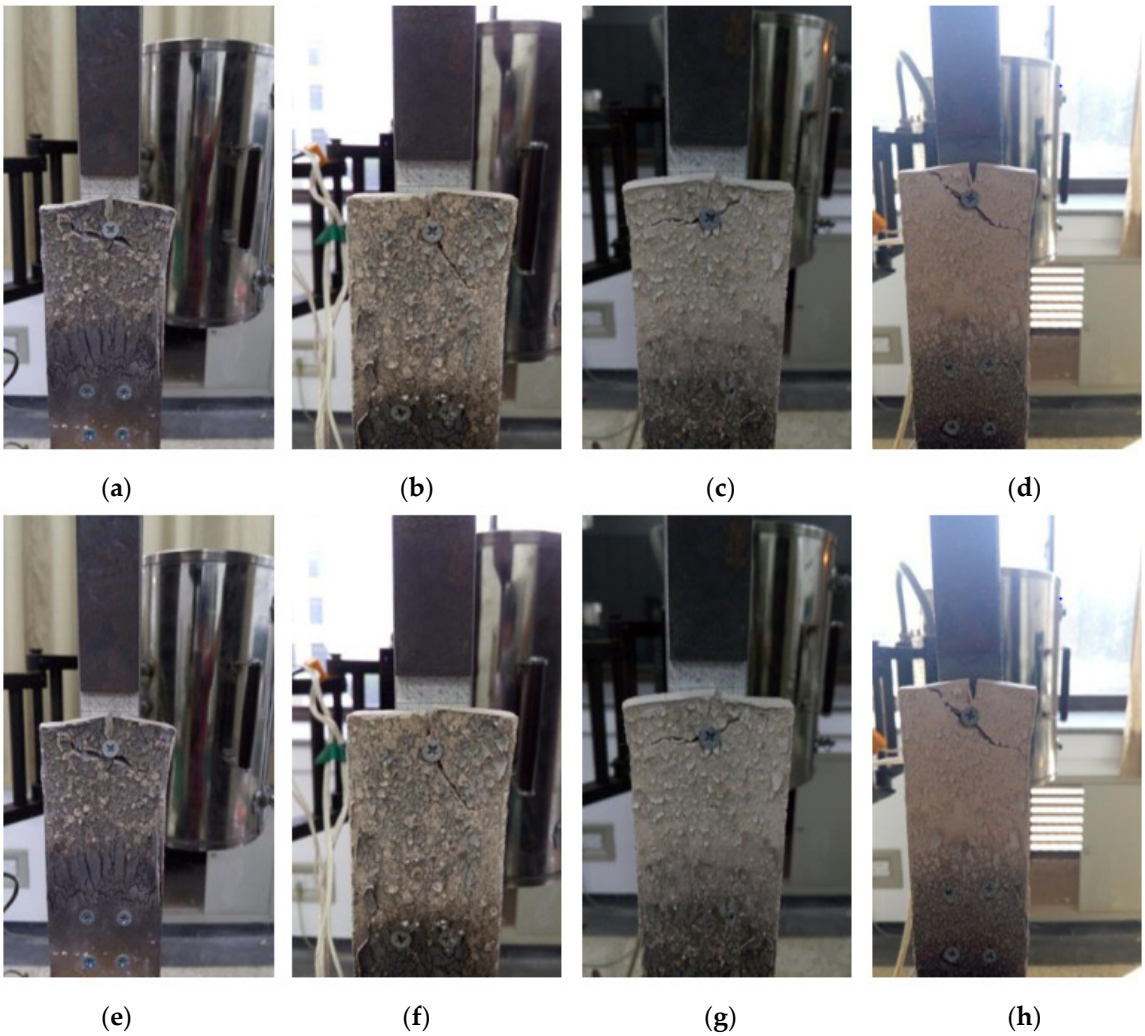

Figure 9. Failure modes of GPB15S series at elevated temperatures: (**a**) 150 °C; (**b**) 200 °C; (**c**) 250 °C; (**d**) 300 °C; (**e**) 350 °C; (**f**) 400 °C; (**g**) 450 °C; and (**h**) 500 °C.

Figure 10. *Cont.*

(**e**) (**f**) (**g**) (**h**)

Figure 10. Failure modes of GPB20D series at elevated temperatures: (**a**) 150 °C; (**b**) 200 °C; (**c**) 250 °C; (**d**) 300 °C; (**e**) 350 °C; (**f**) 400 °C; (**g**) 450 °C; and (**h**) 500 °C.

3.3. Failure Mechanisms

For the connection series with single-layer gypsum sheathing, all of the specimens demonstrated the breaking of the loaded sheathing edge at ambient and elevated temperatures (Figures 6 and 9). In addition, a slight tilting of the screw was found in some specimens in the GBP20S-20 series due to the improved shear strength from increasing the loaded edge distance from 15 mm to 20 mm. However, the screw tilting disappeared beyond 100 °C because of the degenerated shear strength of the connections at elevated temperatures.

For the connection series with double-layer gypsum sheathing, the double length of the screw arm, which is the perpendicular distance from the screw's bugle head to the CFS coupon, resulted in the occurrence of screw tilting at a low shear load. With increasing screw tilt, the loaded sheathing edge suffers additional out-of-plane bending. Therefore, except for the breaking of the loaded sheathing edge, the connection series with the double-layer gypsum sheathing also displayed obvious screw tilting and sheathing flexing fraction at ambient temperature (Figure 7). Again, the screw tilting and sheathing flexing fraction disappear gradually at elevated temperatures (Figure 10) due to the degenerated shear strength.

3.4. Effect of the Loaded Edge Distance

Figure 11 shows the ratio of the test results of the fastener series with a loaded sheathing edge of 15 or 20 mm to those of the series with a loaded sheathing edge of 10 mm at the same temperature. Figure 11a reveals that the connection shear strength increases with increasing loaded edge distance at ambient and elevated temperatures. For the single-layer sheathing connection, the shear strength became approximately 1.4 to 2.1 times of that of GPB10S by increasing the edge distance from 10 to 20 mm; when the loaded edge distance increased from 10 to 15 mm, the shear strength increased by approximately 1.1 to 1.6 times, except at 400 °C. For the double-layer sheathing connection, increasing the loaded edge distance from 10 to 20 mm increased the shear strength by approximately 1.3 to 2.3 times. The shear strength of GPB15D was very close to that of GPB10D from 250 °C to 450 °C. At other temperatures, the shear strength was approximately 1.1 to 1.3 times greater by increasing the loaded edge distance from 10 to 15 mm. Moreover, it should be noticed that the effect of the loaded edge distance on the connection shear strength would become insignificant when it was long enough. In this case, the connection failure mode would likely become screw pull-through.

Although significant scatter existed in the other test results, some basic findings are clear: (a) the absorbed energy of the connection increases with increasing loaded edge distance at ambient and elevated temperatures, as shown in Figure 11b; and (b) the effect of the loaded edge distance on the initial connection stiffness is insignificant at room temperature; the initial stiffness of GPB15D is close to that of GPB10D at elevated temperatures; and for other series, the initial stiffness also increased with increasing loaded edge distance beyond 100 °C, as shown in Figure 11c.

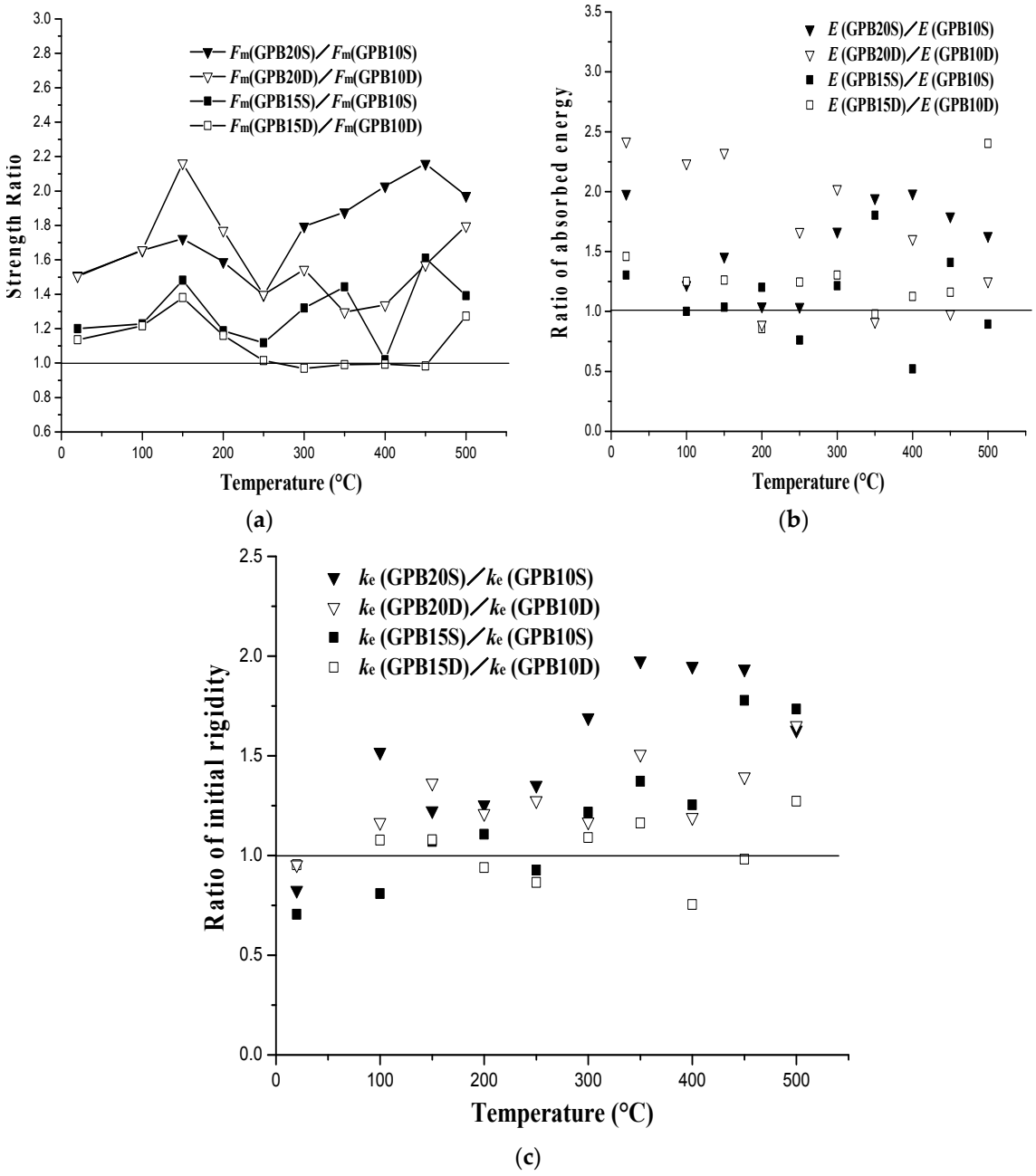

Figure 11. Effect of the loaded edge distance: (**a**) ratio of shear strength; (**b**) ratio of absorbed energy; and (**c**) ratio of initial stiffness.

3.5. Effect of the Double-Layer Gypsum Sheathing

Figure 12 shows the ratio of the test results of the fastener series with double-layer sheathing to those of the series with single-layer sheathing. In Figure 12a, except for the GPB20 series at 400 °C

and GPB15 at 450 °C, the shear strength of the other series increased when replacing the single-layer sheathing with double layers of gypsum plasterboard. Most of the ratios for the shear strength fell between 1.2 and 1.6. In Figure 12b, the absorbed energy capacity of the connection with double layers of gypsum plasterboard was much higher than that of the connection with single-layer sheathing. Most of the ratios for the absorbed energy were above 2.0. Moreover, replacing single-layer gypsum sheathing with a double layer of gypsum plasterboard had an insignificant effect on the initial connection stiffness at ambient temperature, but the effect became favorable beyond 100 °C with an average ratio of approximately 1.5.

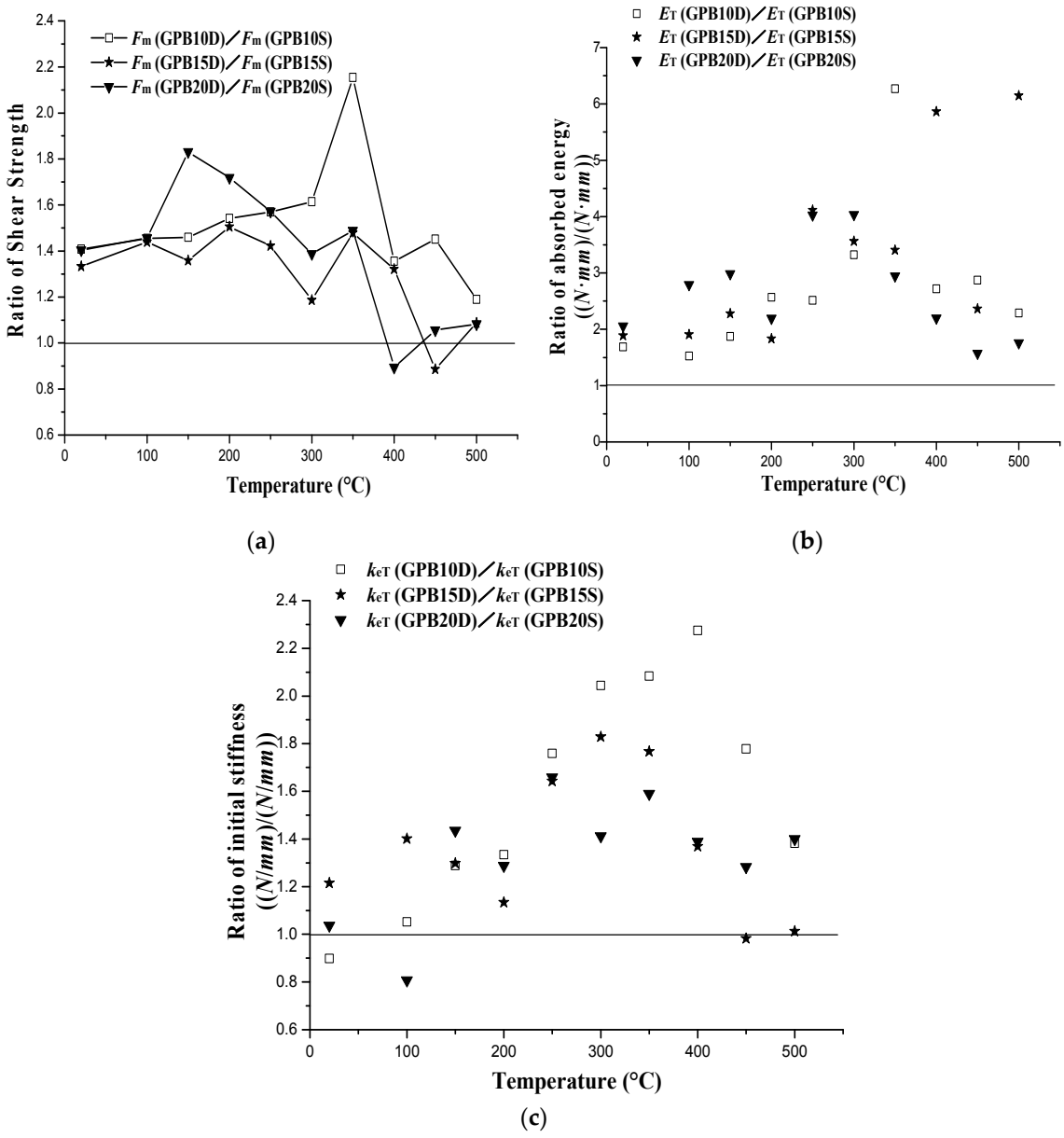

Figure 12. Effect of double-layer gypsum sheathing: (**a**) ratio of shear strength; (**b**) ratio of absorbed energy; and (**c**) ratio of initial stiffness.

4. Design of CFS Screw Connection with Gypsum Sheathing

4.1. Shear Strength Design

Based on the all-steel design method of CFS wall studs in AISI S100-2012 [1], the bearing capacity of a wall stud with small slenderness can be determined by the shear strength of the screw connection with sheathing. In addition, the degeneration of the lateral performance of a CFS wall is usually caused by the shear failure of screw connections [15,16]. The current AISI design manual [25] gives the maximum nominal load per screw connection with gypsum sheathing at ambient temperature. However, the effects of the loaded sheathing edge, double-layer sheathing and elevated temperatures were not yet considered. Therefore, for CFS walls with double-layer gypsum sheathing or increased loaded edge distance, both the axial and lateral design could be overly conservative. This paper recommends including the favorable effects of the loaded sheathing edge and double-layer sheathing on the shear behavior of the screw connection at ambient and elevated temperatures based on reliable construction.

A unified prediction formula for F_{mT} was proposed by non-linear regression, as shown in Equation (1), where d represents the loaded edge distance; α is the coefficient that considers the effect of double-layer gypsum sheathing at ambient temperature, as shown in Equations (2) and (3); and R_{mT} is the reduction factor of shear strength, defined as the ratio of the shear strength at elevated temperatures to that at ambient temperature. R_{mT} is developed by the multi-segment polynomials, as shown in Equation (4). The values of the coefficients in Equation (4) are given in Table 3. Based on the previous thermal physical experiments of fire-resistant gypsum plasterboard at elevated temperatures [21], the dehydration of gypsum plasterboard (CaSO4·2H2O) occurred from approximately 85 °C to 160 °C. Therefore, R_{mT} is assumed to be 1.0 for temperatures below 80 °C in Table 3. The R_{mT} predicted by Equation (4) is in good agreement with the values obtained from the present experiments, as shown in Figure 13.

$$F_{mT} = 316e^{0.04d} \cdot \alpha \cdot R_{mT}, \quad 10 \le d \le 20 \text{ mm} \tag{1}$$

where the units of F_{mT} are N.

For single-layer gypsum sheathing,

$$\alpha = 1.0 \tag{2}$$

For double-layer gypsum sheathing,

$$\alpha = 0.0028d^2 - 0.085d + 1.98, \quad 10 \le d \le 20 \text{ mm} \tag{3}$$

$$R_{mT} = aT^2 + bT + c \tag{4}$$

where a, b and c are the coefficients of Equation (4).

Figure 14 compares the values of F_{mT} predicted by Equation (1) to those obtained from the present 200 experiments. The average ratio of the predicted F_{mT} to the experimental results is 98.8%, and the Pearson product-moment correlation coefficient is 0.995. Thus, Equation (1) is able to accurately evaluate the shear strength of the screw connection with single- or double-layer gypsum sheathing and different edge distances at ambient and elevated temperatures. In structural engineering design, if the loaded edge distance exceeds 20 mm, Equation (1) can still be used with the loaded edge distance of 20 mm to obtain a conservative prediction of the shear strength of the screw connection, and a factor of safety [25] can be applied to the maximum allowable axial strength of the screw connection, as shown in Equation (5).

$$F_{aT} = F_{mT}/\Omega \tag{5}$$

where F_{aT} is the maximum allowable axial strength of the screw connection with sheathing and Ω is the factor of safety for the screw connection [25].

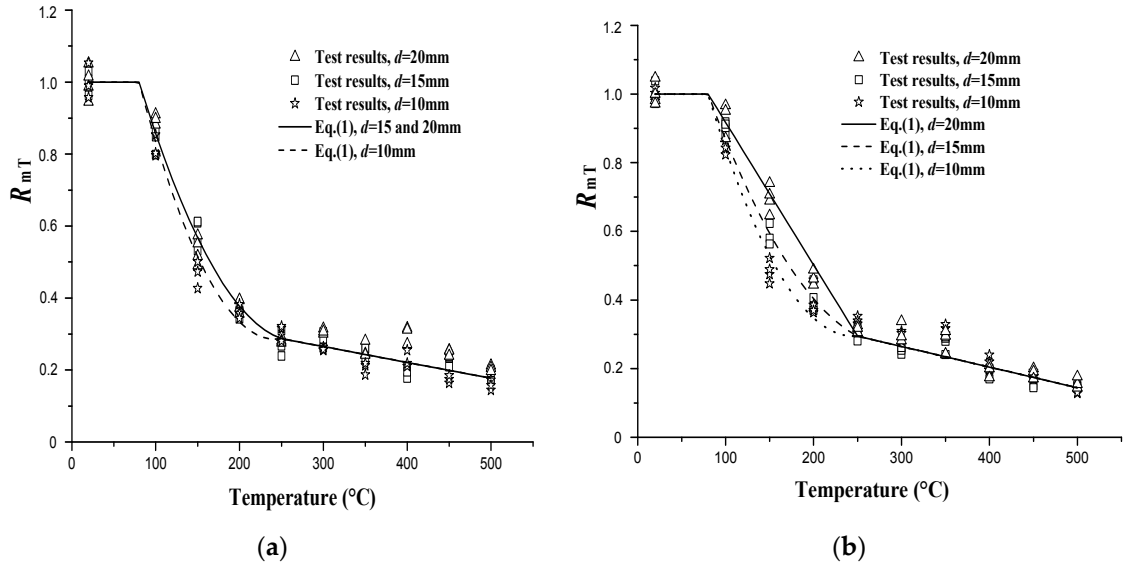

Figure 13. Comparison of R_{mT} obtained from Equation (4) and experimental results: (**a**) single-layer gypsum; and (**b**) double-layer gypsum sheathing.

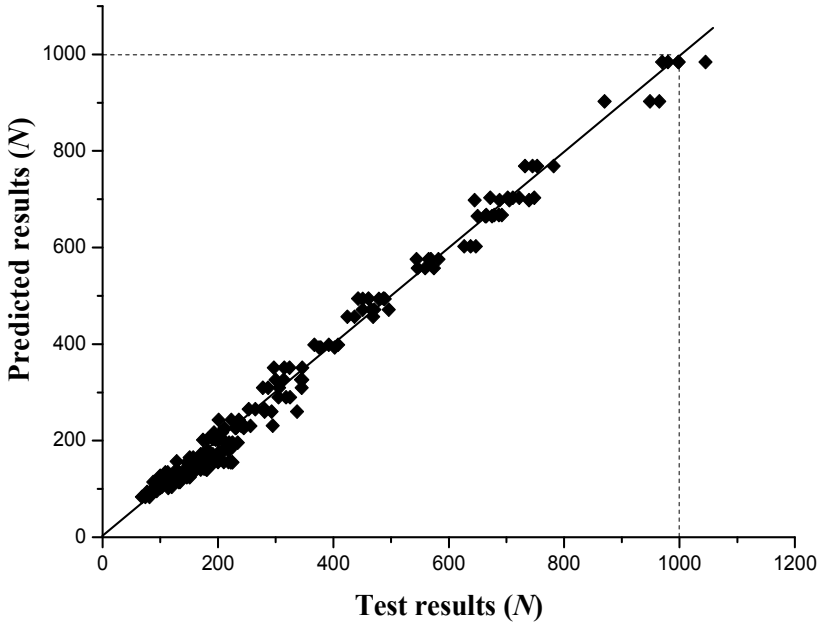

Figure 14. Predicted shear strength compared to experimental results.

Table 3. Values of Coefficients in Equation (4).

Sheathing	Temperature (°C)	Edge Distance of 10 mm			Edge Distance of 15 mm			Edge Distance of 20 mm		
		a	***b***	***c***	***a***	***b***	***c***	***a***	***b***	***c***
Single-layer gypsum	$20 \leq T \leq 80$	0	0	1	0	0	1	0	0	1
	$80 < T \leq 250$	2.73×10^{-5}	-1.32×10^{-2}	1.881	2×10^{-5}	-1.08×10^{-2}	1.737	2×10^{-5}	-1.08×10^{-2}	1.737
	$250 < T \leq 500$	0	-4.4×10^{-4}	3.97×10^{-1}	0	-4.4×10^{-4}	3.97×10^{-1}	0	-4.4×10^{-4}	3.97×10^{-1}
Double-layer gypsum	$20 \leq T \leq 80$	0	0	1	0	0	1	0	0	1
	$80 < T \leq 250$	2.58×10^{-5}	-1.266×10^{-2}	1.847	1.65×10^{-5}	-9.6×10^{-3}	1.663	0	-4.15×10^{-3}	1.332
	$250 < T \leq 500$	0	-6×10^{-4}	4.445×10^{-1}	0	-6×10^{-4}	4.445×10^{-1}	0	-6×10^{-4}	4.445×10^{-1}

4.2. Other Parameters

Some other screw connection parameters were also considered, including k_{eT}, Δ_{mT} and Δ_{uT}. Because the scatter is significant, fitting these parameters focused on the simplicity of operation and conservation instead of accuracy. The prediction formula of the initial screw connection stiffness at ambient and elevated temperatures is given in Equation (6). R_{kT} is the reduction factor of the initial stiffness defined as the ratio of the initial stiffness at elevated temperatures to that at ambient temperature. The values of R_{kT} are shown in Table 4, and they did not consider the sudden increase in initial stiffness at 100 °C (Tables 1 and 2). Figure 15 compares the predicted R_{kT} to the test results at ambient and elevated temperatures. In most cases, the k_{eT} values obtained from Equation (6) are conservative and easy for operation.

$$k_{eT} = R_{kT} \cdot 1000 \tag{6}$$

where the units of k_{eT} are N/mm.

Equation (7) is the prediction formula of Δ_{mT}, which takes the larger value of of F_{mT}/k_{eT} and $\alpha_1 \cdot \Delta_{1T}$. F_{mT} and k_{eT} can be obtained from Equations (1) and (6), respectively. Δ_{1T} is the predicted displacement corresponding to F_{mT} for the screw connection with single-layer gypsum sheathing at T °C. Figure 16 gives the values of the predicted Δ_{1T} based on the present experiments. α_1 is the coefficient that considers the effect of double-layer gypsum sheathing on Δ_{mT}, as shown in Equations (8) and (9). As shown in Table 2, the test results of Δ_{mT} for the connection series with double-layer gypsum sheathing and a loaded edge distance of 20 mm were much lower than those of the series with double-layer gypsum sheathing and a loaded edge distance of 15 or 10 mm for temperatures beyond 250 °C. This phenomenon seems unusual, and it was not considered in Equation (9).

$$\Delta_{mT} = \max(F_{mT}/k_{eT}, \alpha_1 \cdot \Delta_{1T}) \tag{7}$$

where the units of Δ_{mT} and Δ_{1T} are mm.

For single-layer gypsum sheathing,

$$\alpha_1 = 1.0 \tag{8}$$

For double-layer gypsum sheathing,

$$\alpha_1 = 1.3 \tag{9}$$

In addition, the prediction formula of Δ_{uT} was also given, as shown in Equation (10). α_2 is the additional coefficient that considers the effect of double-layer gypsum sheathing on Δ_{uT} at elevated temperatures, as shown in Equations (11) and (12).

$$\Delta_{uT} = 1.5 \cdot \alpha_2 \cdot \Delta_{mT} \tag{10}$$

where the units of Δ_{uT} are mm.

For single-layer gypsum sheathing,

$$\alpha_2 = 1.0 \tag{11}$$

For double-layer gypsum sheathing,

$$\alpha_2 = 1.0,\ T \leq 200\,^{\circ}\mathrm{C} \text{ and } \alpha_2 = 1.6,\ T > 200\,^{\circ}\mathrm{C} \tag{12}$$

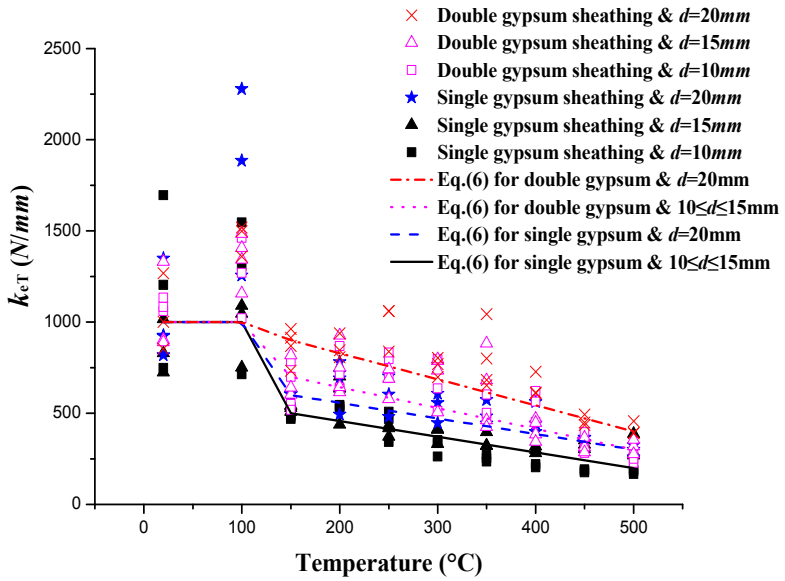

Figure 15. Predicted initial stiffness compared to the experimental results.

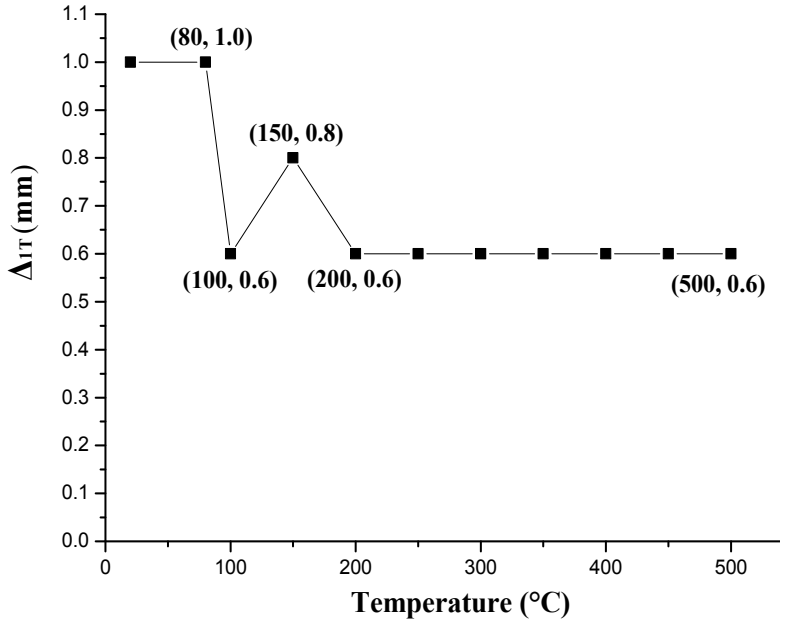

Figure 16. Predicted values of Δ_{1T}.

Table 4. Values of R_{kT} in Equation (6).

Sheathing	Edge Distance (mm)	Temperature (°C)		
		≤100 °C	150 °C	500 °C
Single-layer gypsum	$10 \leq d \leq 15$	100%	50%	20%
	$d \geq 20$	100%	60%	30%
Double-layer gypsum	$10 \leq d \leq 15$	100%	70%	30%
	$d \geq 20$	100%	90%	40%

Note: Values of R_{kT} at other temperatures can be obtained by linear interpolation.

4.3. Load–Displacement Model of the Screw Connections

The load–displacement curves of the screw connections at ambient and elevated temperatures are important input parameters for the elaborate simulation of the mechanical performance of CFS walls at ambient temperature or in fire conditions. A four-line degradation model was adopted by Ye et al. [9] to predict the load–displacement curve of the connection at ambient temperature. However, the four-line degradation model has at least eight parameters, and it is not easy to operate. The Foschi exponential model [10] can also be used to describe the load–displacement characteristic of the connection at room temperature, but it becomes inconvenient at elevated temperatures due to its irregular change in parameters. Based on the above prediction formulas for F_{mT}, K_{eT}, Δ_{mT} and Δ_{uT}, a simplified load–displacement model with the post-peak branch was developed for the screw connection at both ambient and elevated temperatures, as shown in Equation (13). The pre-peak branch of the load–displacement model was obtained by modifying the Ramberg-Osgood model [26]. The post-peak branch showed a linear decrease from Δ_{mT} to Δ_{uT}. To simplify the operation, the exponent A in Equation (13) was given a constant value for the fastener series with the same configuration and elevated temperature, as shown in Table 5.

$$\Delta_T = \begin{cases} (\Delta_{mT} - \frac{F_{mT}}{k_{eT}})(\frac{F_T}{F_{mT}})^A + \frac{F_T}{k_{eT}}, & F_T \le F_{mT} \text{ and } \Delta_T \le \Delta_{mT} \\ 5\Delta_{uT} - 4\Delta_{mT} - \frac{5\Delta_{uT} - 5\Delta_{mT}}{F_{mT}} F_T, & \Delta_{mT} < \Delta_T \le \Delta_{uT} \text{ and } F_{uT} \le F_T < F_{mT} \end{cases} \quad (13)$$

where Δ_T is the connection displacement at T °C and F_T is the connection shear load at T °C.

Taking the screw connection with the loaded edge distance of 15 mm as an example, Figure 17 compares the load–displacement curves predicted by Equation (13) to the experimental results. All of the key parameters in Equation (13), including F_{mT}, K_{eT}, Δ_{mT} and Δ_{uT}, were obtained from the present prediction formulas (Equation (1) through Equations (4) and (6) through Equation (12)). The present load–displacement model can provide a reasonable estimate of the load–displacement response of the screw connection at ambient and elevated temperatures with acceptable accuracy and simple operation. In some cases, visible differences exist between the predicted curves and the experimental results, such as the load–displacement curve of the screw connection with single-layer gypsum sheathing at 500 °C (Figure 17a). This difference is due to the errors of the predicted K_{eT}, Δ_{mT} and Δ_{uT}, which are inevitable due to the significant scatter of these parameters in the experiments.

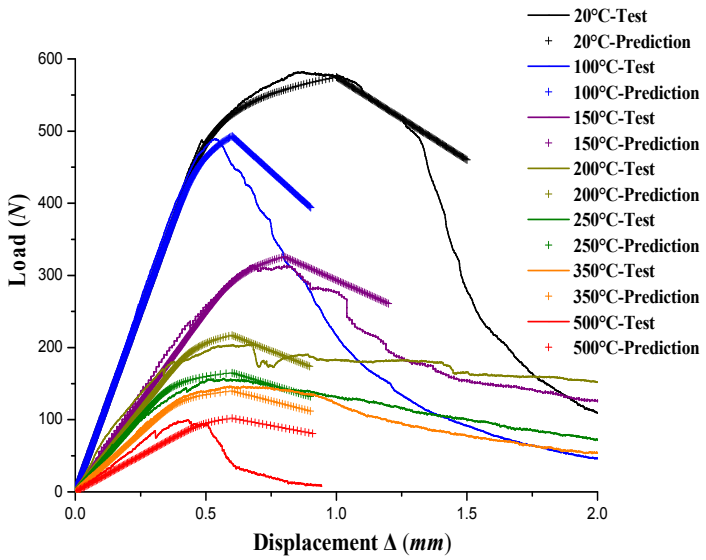

(a)

Figure 17. *Cont.*

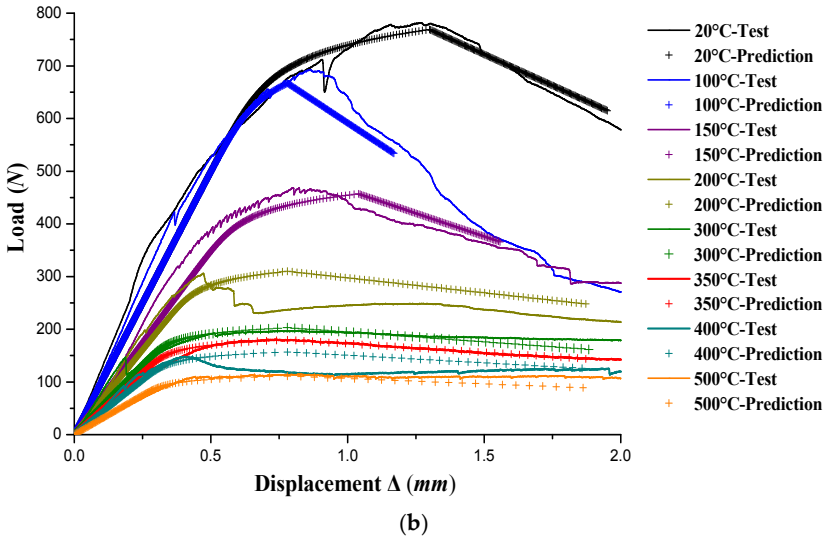

Figure 17. Comparison of the predicted load–displacement curves to the experimental results: (**a**) screw connection with single-layer gypsum sheathing and a loaded edge distance of 15 mm; and (**b**) screw connection with double-layer gypsum sheathing and a loaded edge distance of 15 mm.

Table 5. Values of the exponent A in Equation (13).

Sheathing	Edge Distance (mm)	A
Single-layer gypsum	$d = 10$	4
	$d \geq 15$	18
Double-layer gypsum	$d = 10$	10
	$d \geq 15$	18

Note: If d lies between 10 and 15 mm, the values of A can be obtained by linear interpolation.

5. Conclusions

This paper reported a detailed study of 200 monotonic tests of CFS screw connections with gypsum sheathing at both ambient and elevated temperatures. Three loaded edge distances and single- or double-layer gypsum sheathing were taken into account in the experiments. The following conclusions are drawn from this work:

(1) The failure characteristic of the screw connections with double-layer gypsum sheathing in shear was different from that of single-layer gypsum sheathing connections at ambient temperature, and it could be described as the breaking of the loaded sheathing edge combined with significant screw tilting and loaded sheathing edge flexing fracture. The screw tilting and loaded sheathing edge flexing fracture disappear gradually at elevated temperatures.

(2) Compared to the shear strength at ambient temperature, the shear strength of screw connection decreased sharply at 150 °C and 200 °C due to the gypsum dehydration and gradually declined from 250 °C to 500 °C.

(3) The initial screw connection stiffness seems irrelevant to the loaded edge distance of more than 10 mm and single- or double-layer gypsum sheathing at ambient temperature. The shear strength and absorbed energy of the screw connection were significantly enhanced by increasing the loaded edge distance from 10 mm to 20 mm or replacing the single-layer gypsum sheathing with double-layer sheathing at both ambient and elevated temperatures.

(4) The shear strength of screw connection could not be linearly superposed by the number of layers of gypsum sheathing because the shear strength of screw connection with double-layer gypsum sheathing is less than twice the screw connection strength with single-layer gypsum sheathing at ambient and elevated temperatures.

(5) A unified design formula for the screw connection shear strength at ambient and elevated temperatures was proposed with sufficient accuracy, and it takes into account the effect of the loaded edge distance and double-layer gypsum sheathing. In addition, a simplified load–displacement model with the post-peak branch was developed to evaluate the load–displacement response of the screw connection with different loaded edge distances and single- or double-layer gypsum sheathing at ambient and elevated temperatures.

Acknowledgments: This research was supported by the National Natural Science Foundation of China (Grant No. 51508088); Natural Science Foundation of Jiangsu Province of China (Grant No. BK20150605); the Priority Academic Program Development of Jiangsu Higher Education Institutions, Key Laboratory of Building Fire Protection Engineering and Technology of MPS (Grant No. KFKT2015ZD05); Jiangsu Key Laboratory of Environmental Impact and Structural Safety in Engineering (Grant No. JSKL2014K04); and Jiangsu Key Laboratory of Structure Engineering (Grant No. ZD1402). The authors thank Xu Zhihong and Dong Xuehua for their kind assistance during the experiments.

Author Contributions: Wei Chen contributed to design and conduct the experiments, perform the data analyses and write the manuscript; Jihong Ye contributed to the conception of the study; Tao Chen contributed to provide the test device and discuss the results.

Conflicts of Interest: The authors declare no conflict of interest.

References

1. American Iron and Steel Institute. *AISI-S100-12 (North American Specification for the Design of Cold-Formed Steel Structural Members)*; American Iron and Steel Institute: Washington, DC, USA, 2012.
2. Yu, W.W.; LaBoube, R.A. *Cold-Formed Steel Design*, 4th ed.; John Wiley & Sons: Hoboken, NJ, USA, 2010.
3. Serrette, R.L.; Encalada, J.; Juadines, M.; Nguyen, H. Static racking behavior of plywood, OSB, gypsum, and fiberboard walls with metal framing. *J. Struct. Eng. ASCE* **1997**, *123*, 1079–1086. [CrossRef]
4. Fülöp, L.A.; Dubina, D. Design criteria for seam and sheeting to framing connections of cold-formed steel shear panels. *J. Struct. Eng.* **2006**, *132*, 582–590. [CrossRef]
5. Nithyadharan, M.; Kalyanaraman, V. Experimental study of screw connections in CFS-calcium silicate board wall panels. *Thin Walled Struct.* **2011**, *49*, 724–731. [CrossRef]
6. Fiorino, L.; Della Corte, G.; Landolfo, R. Experimental tests on typical screw connections for cold-formed steel housing. *Eng. Struct.* **2007**, *29*, 1761–1773. [CrossRef]
7. Peterman, K.D.; Nakata, N.; Schafer, B.W. Hysteretic characterization of cold-formed steel stud-to-sheathing connections. *J. Constr. Steel Res.* **2014**, *101*, 254–264. [CrossRef]
8. Swensen, S.; Deierlein G, G.; Miranda, E. Behavior of screw and adhesive connections to gypsum wallboard in wood and cold-formed steel-framed Wallettes. *J. Struct. Eng. ASCE* **2015**, *142*, E4015002-1–E4015002-11. [CrossRef]
9. Ye, J.H.; Wang, X.X.; Zhao, M.Y. Experimental study on shear behavior of screw connections in CFS sheathing. *J. Constr. Steel Res.* **2016**, *121*, 1–12. [CrossRef]
10. Foschi, R.O. Load-slip characteristics of nails. *Wood Sci.* **1974**, *7*, 69–76.
11. Dowell, R.K.; Seibel, F.; Wilson, E.L. Pivot hysteresis model for reinforced concrete members. *ACI Struct. J.* **1998**, *95*, 607–617.
12. Chen, W.; Ye, J.H.; Bai, Y.; Zhao, X.L. Improved fire resistant performance of load bearing cold-formed steel interior and exterior wall systems. *Thin Walled Struct.* **2013**, *73*, 145–157. [CrossRef]
13. Chen, W.; Ye, J.H.; Bai, Y.; Zhao, X.L. Full-Scale fire experiments on load-bearing cold-formed steel walls lined with different panels. *J. Constr. Steel Res.* **2012**, *79*, 242–254. [CrossRef]
14. Sakumoto, Y.; Hirakawa, T.; Masuda, H.; Nakamura, K. Fire resistance of walls and floors using light-gauge steel shapes. *J. Struct. Eng.* **2003**, *129*, 1522–1530. [CrossRef]
15. Wang, X.X.; Ye, J.H. Cyclic testing of two- and three-story CFS shear-walls with reinforced end studs. *J. Constr. Steel Res.* **2016**, *121*, 13–28. [CrossRef]
16. Ye, J.H.; Wang, X.X.; Jia, H.Y.; Zhao, M.Y. Cyclic performance of cold-formed steel shear walls sheathed with double-layer wallboards on both sides. *Thin Walled Struct.* **2015**, *92*, 146–159. [CrossRef]
17. American Iron and Steel Institute. *AISI-S400-15 (North American Standard for Seismic Design of Cold-Formed Steel Structural Systems)*; American Iron and Steel Institute: Washington, DC, USA, 2015.

18. Lu, W.; Mäkeläinen, P.; Outinen, J.; Ma, Z. Design of screwed steel sheeting connection at ambient and elevated temperatures. *Thin Walled Struct.* **2011**, *49*, 1526–1533. [CrossRef]
19. Yan, S.; Young, B. Screwed connections of thin sheet steels at elevated temperatures—Part I: Steady state tests. *Eng. Struct.* **2012**, *35*, 234–243. [CrossRef]
20. Cai, Y.C.; Young, B. Behavior of cold-formed stainless steel single shear bolted connections at elevated temperatures. *Thin Walled Struct.* **2014**, *75*, 63–75. [CrossRef]
21. Chen, W.; Ye, J.H.; Bai, Y.; Zhao, X.L. Thermal and mechanical modeling of load-bearing cold-formed steel wall systems in fire. *J. Struct. Eng.* **2014**, *140*, 1–13. [CrossRef]
22. Gunalan, S.; Mahendran, M. Finite element modelling of load bearing cold-formed steel wall systems under fire conditions. *Eng. Struct.* **2013**, *56*, 1007–1027. [CrossRef]
23. China Institute of Building Standard Design & Research. *Technical Specification for Low-Rise Cold-Formed Thin-Walled Steel Buildings*; China Architecture & Building Press: Beijing, China, 2012. (In Chinese)
24. American Society for Testing and Materials. *ASTM Standard E2126-11 (Standard Test Methods for Cyclic (Reversed) Load Test for Shear Resistance of Vertical Elements of the Lateral Force Resisting Systems for Buildings)*; American Society for Testing and Materials: West Conshohocken, PA, USA, 2011.
25. American Iron and Steel Institute. *AISI-S211-07 (North American Standard for Cold-Formed Steel Framing—Wall Stud Design)*; American Iron and Steel Institute: Washington, DC, USA, 2007.
26. Ramberg, W.; Osgood, W.R. Description of Stress-Strain Curves by Three Parameters. Patent NACA-TN-902, 1 July 1943.